Journal of Power Sources 262 (2014) 451–456

Contents lists available at ScienceDirect

Journal of Power Sources

journal homepage: www.elsevier.com/locate/jpowsour

Degradation of nickel–yttria-stabilized zirconia anode in solid oxide fuel cells under changing temperature and humidity conditions

Yi-Hsuan Lee, Hiroki Muroyama, Toshiaki Matsui, Koichi Eguchi*

Department of Energy and Hydrocarbon Chemistry, Graduate School of Engineering, Kyoto University, Nishikyo-ku, Kyoto 615-8510, Japan

HIGHLIGHTS

- Long-term stability was investigated at 1000–1200 °C under the OCV condition.
- The microstructural change in the Ni–YSZ anode was quantitatively analyzed.
- A mechanism of Ni aggregation under high humidity atmosphere was suggested.

ARTICLE INFO

Article history:
Received 10 January 2014
Received in revised form
21 February 2014
Accepted 12 March 2014
Available online 31 March 2014

Keywords:
Solid oxide fuel cells
Ni–yttria-stabilized zirconia
Anode
Sintering
Microstructure
FIB–SEM

ABSTRACT

The performance degradation of Ni–yttria-stabilized zirconia (Ni–YSZ) cermet anode was measured by impedance spectroscopy at 1000–1200 °C and humidity atmospheres under the open circuit condition in SOFCs. More significant crack formation can be observed at 1200 °C under 40% H_2O–60% H_2 atmosphere. This crack formation gave rise to interruption of the ionic and electronic conduction path in the in-plane direction of anode layer, resulting in performance deterioration of anode. Focused ion beam-scanning electron microscopy (FIB–SEM) analyses were conducted for the anode layers, and then the 3D microstructures of Ni–YSZ anode were reconstructed. According to analysis of these data, the particle size of Ni was grown to the larger under higher temperature and humidity condition, accompanying with increase of isolated Ni-phase and the reduction of triple phase boundary (TPB) length.

1. Introduction

Solid oxide fuel cells (SOFCs) are one of the attractive power generation systems due to the low emission, high efficiency, and fuel flexibility at high temperatures [1,2]. The Ni–yttria-stabilized zirconia (Ni–YSZ) cermet is the most common material of anode. The electrochemical reaction between oxide ion, hydrogen, and electron only takes place at triple-phase boundaries (TPB) in Ni–YSZ anode [3–5]. Therefore, the anode is porous to allow the hydrogen to flow towards the electrolyte, and transport electron and oxide ions in the Ni and YSZ, respectively. The YSZ component serves to inhibit the sintering of the Ni particles and to provide a close thermal expansion coefficient for Ni–YSZ cermet to that of the YSZ electrolyte. Moreover, with mixing Ni and YSZ, the TPB length can extend efficiently to improve cell performance. However, the performance of the Ni–YSZ anode cermet sometimes degraded after long-term operation by supplying humid hydrogen [6–10].

Many studies have been devoted to clarify the degradation factors for Ni–YSZ anode during long-term operation. Simwonis et al. reported that the electrical conductivity of Ni–YSZ cermet decreased at 1000 °C during supply of 4% H_2–3% H_2O–93% Ar for 4000 h [9]. The size of YSZ particles shows no changes before and after treatments. On the other hand, the sintering behavior of Ni particles has been observed. Tanasini et al. have shown that the polarization resistance increased after operation at a constant current density of 0.6 A cm^{-2} at 850 °C for 1000 h with a supply of 97% H_2–3% H_2O, resulting from Ni coarsening [10]. One possible reason for the performance degradation was growth of Ni-particles size in association with a reduction of TPB length [10].

In addition, the sintering of Ni particles became apparent with increasing temperature and humidity [11–13]. The migration mechanism of Ni particles has been considered to proceed via (1) surface diffusion and/or (2) transportation in the gas phase. The

* Corresponding author. Tel.: +81 75 383 2519; fax: +81 75 383 2520.
E-mail address: eguchi@scl.kyoto-u.ac.jp (K. Eguchi).

http://dx.doi.org/10.1016/j.jpowsour.2014.03.031
0378-7753/

surface diffusion is affected by temperature primarily. In the case of transportation in the gas phase especially under humidity atmospheres, according to thermodynamic data, Ni species i.e. $Ni(OH)_{2(g)}$ is more volatile than $Ni_{(g)}$ at 950 °C over *ca.* 20% H_2O concentration [12]. Additionally, it was shown that the equilibrium pressure of Ni-hydroxide complexes is more sensitive to the H_2O concentration [13]. Therefore, the coarsening of Ni particles due to increase of humidity may be associated with the partial pressure of Ni-hydroxide complexes. However, the quantitative relationship between the sintering of Ni particles and performance deterioration has not been elucidated sufficiently.

Recently, the quantitative measurements of SOFC electrode microstructure have been conducted with focused ion beam–scanning electron microscopy (FIB–SEM) [14–18]. In this study, the Ni–YSZ anode of cells were treated at 1100 °C and 1200 °C at open circuit condition for 50 h under highly humidified hydrogen atmospheres to accelerate the microstructural changes of cermet anode. After the heat treatments, samples were analyzed by FIB–SEM, and their microstructural change was quantified to clarify the degradation factors.

2. Experimental

The NiO–YSZ powder with a volumetric ratio of Ni:YSZ = 50:50 and a perovskite-type oxide of $(La_{0.8}Sr_{0.2})_{0.97}MnO_3$ (LSM) powder were used for the anode and cathode, respectively. The Ni–YSZ cermet was prepared from NiO (Wako Pure Chemical Industries) and YSZ powders (8 mol% Y_2O_3–ZrO_2, Tosoh). The mixture of NiO and YSZ was heat-treated at 1200 °C for 5 h. An LSM power was prepared from corresponding metal acetates, and calcined at 900 °C for 5 h. The resulting powder of each electrode material was mixed with polyethylene glycol (Wako Pure Chemical Industries) to form slurry. The NiO–YSZ cermet slurry was screen-printed on one face of the YSZ disk (Tosoh, thickness: 500 μm, diameter: 24 mm) at the center, followed by the calcination at 1400 °C for 5 h (anode thickness: *ca.* 40 μm). The cathode slurry was coated in the same way on the other face of the disk and subsequently heated at 1150 °C for 5 h. The fabricated cell was sandwiched by alumina tubes with Pyrex glass seals, as is shown in previous paper [19].

The change in anodic performance was investigated by holding under the open-circuit condition at 1000 °C, 1100 °C, and 1200 °C for 50 h. A gaseous mixture of 10% H_2O–90% H_2 or 40% H_2O–60% H_2 was supplied to the anode with a flow rate of 100 ml min^{-1}. During these operations, pure oxygen was fed to the cathode as an oxidant with a flow rate of 100 ml min^{-1}. The Cell Test system (Solarton Analytical, potentiostat/galvanostat 1470E and frequency response analyzer 1455A) was used for the electrochemical impedance measurement.

After the evaluation of cell performance, the structural change in Ni–YSZ anode was observed by a dual-beam focused ion beam-scanning electron microscope (FIB–SEM, Nvision 40, Carl Zeiss–SIINT) equipped with an energy dispersive X-ray spectrometer (EDX, Oxford). The sample was infiltrated with epoxy resin, and then the anode cross-section of SEM images (*x*–*y* plane as Fig. 1) was observed. Two dimensional SEM pictures were collected along the *z*-direction by milling-and-see operation [20]. The 3D microstructure of anode was reconstructed in a computational field (Fig. 1). The more detailed description of analysis using a FIB–SEM is reported by Iwai et al. [20]. In this study, the microstructural parameters were quantitatively analyzed; volume fraction, size distribution of particles, ratio of isolated-Ni phase, and triple phase boundary (TPB) length. The particle size distribution of each phase was evaluated by the line intercept method. The TPB length was calculated by the volume expansion method [20].

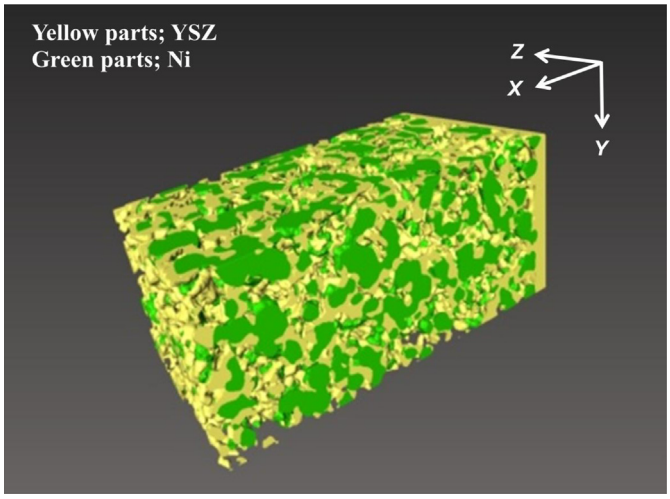

Fig. 1. 3D reconstructed Ni (green) and YSZ (yellow) phase in anode. (For interpretation of the references to color in this figure legend, the reader is referred to the web version of this article.)

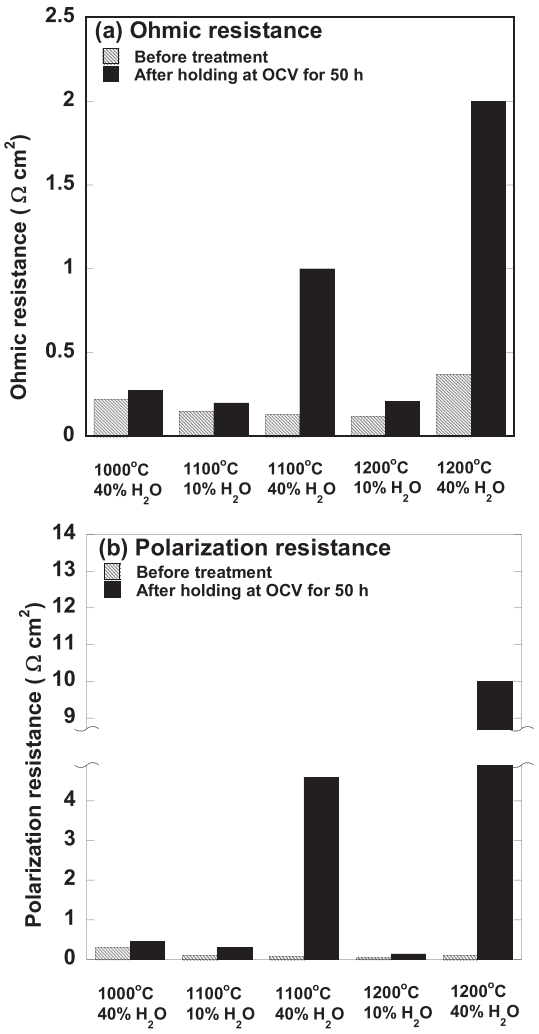

Fig. 2. (a) Ohmic and (b) polarization resistances of anode before and after holding under the OCV for 50 h at 1000 °C–1200 °C with a supply of 10% H_2O–90% H_2 and 40% H_2O–60% H_2.

3. Results and discussion

3.1. Degradation of anode performance at high temperature and humidity

The cell performance was examined by impedance measurement with a supply of 10% H_2O–90% H_2 or 40% H_2O–60% H_2 to the anode at 1000 °C–1200 °C. The ohmic and polarization resistances of Ni–YSZ at open-circuit condition before and after heat-treatments are summarized in Fig. 2. No significant changes in both resistive components were observed in 10% H_2O–90% H_2 even at 1100 °C and 1200 °C. On the other hand, the resistances increased dramatically during the heat-treatment with 40% H_2O–60% H_2 at 1100 °C and 1200 °C, though the anode performance was scarcely deteriorated at 1000 °C. The deterioration was more remarkable at 1200 °C. These results indicated that performance degradation of Ni–YSZ was accelerated by higher humidity and temperature.

3.2. Microstructure change with degradation

The surface and cross-section of Ni–YSZ anodes were observed at low magnification by SEM. Fig. 3(a) and (b) shows the surfaces of anode kept at 1100 °C in 10% H_2O–90% H_2 and 40% H_2O–60% H_2, respectively. Fine cracks were on the surface of anode heat-treated at lower humidity, while annealing in highly humidified atmosphere resulted in the formation of significant crack over the anode surface. The crack formation should result from migration and growth of Ni particles. Fig. 4(a) and (b) shows the surface and cross section of Ni–YSZ anode exposed to 40% H_2O–60% H_2 at 1200 °C for 50 h. Comparing with the sample treated at 1100 °C, more significant cracks were observed on the surface. From the cross-sectional image, the generation of crack was from the anode surface to the interface with YSZ electrolyte, which implies that the Ni–YSZ anode was divided into several island-like parts. The structure will interrupt the ionic and electronic conductions in the in-plane direction of anode layer. Therefore, the reduction of reaction sites and conduction path resulted in the severe degradation of anode performance at 1200 °C under the highly-humidified condition. Hereafter, the anode microstructure was quantitatively analyzed by FIB–SEM.

Table 1 shows the volume fractions of each phase evaluated from the reconstructed Ni–YSZ anodes. Because the volume ratio of Ni to YSZ for all samples was comparable to the nominal composition of Ni:YSZ = 50:50, the series of anode reconstruction and computational analysis were reliable. Fig. 5 displays the size distributions of YSZ particles, Ni particles, and pore in the Ni–YSZ anodes before and after the heat-treatments with a supply of 10% H_2O–90% H_2 and 40% H_2O–60% H_2 at 1000, 1100, and 1200 °C. The size of the YSZ particles was unchanged by the treatment, indicating that the performance degradation was not induced by the

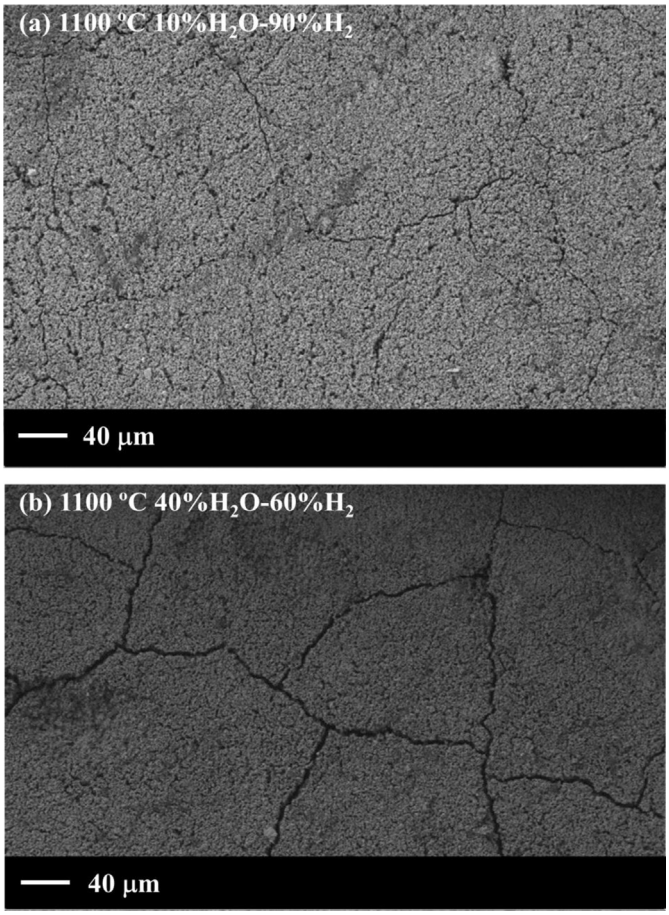

Fig. 3. Secondary electron images for Ni–YSZ surface after holding at OCV for 50 h with a supply of (a) 10% H_2O–90% H_2 at 1100 °C, (b) 40% H_2O–60% H_2 at 1100 °C.

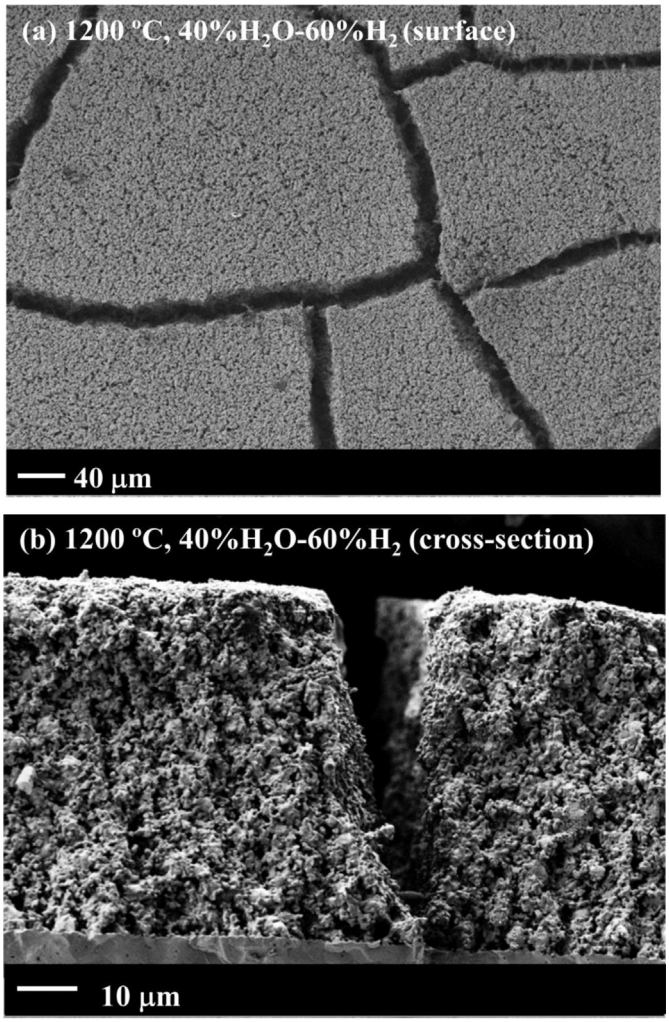

Fig. 4. Secondary electron images for Ni–YSZ (a) surface and (b) cross section after holding at OCV for 50 h with a supply of 40% H_2O–60% H_2 at 1200 °C.

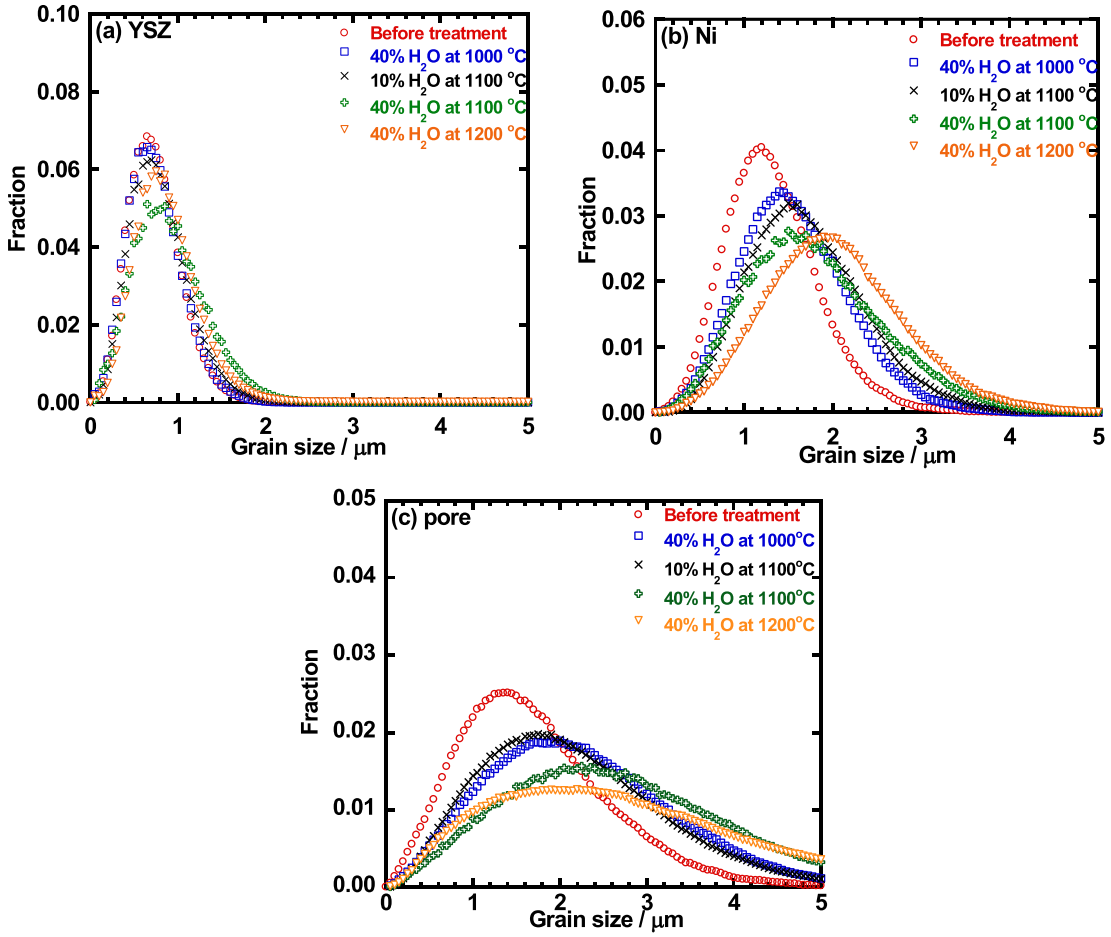

Fig. 5. Size distribution of (a) YSZ particles, (b) Ni particles, and (c) pore in the Ni–YSZ anode cermet before and after holding at OCV with a supply of 10% H_2O–90% H_2 and 40% H_2O–60% H_2 at 1000 °C, 1100 °C, and 1200 °C for 50 h.

particle size change of YSZ. In contrast, the peak of size distribution of Ni particles shifted to large size under high humidity and temperature conditions, suggesting that the sintering of Ni particles contributed to the degradation of anode performance. In addition, the increment of pore sizes was resulted from the Ni particle aggregation. Such a phenomenon has been observed with a supply of 3% H_2O–4% H_2–93% Ar atmosphere at 1000 °C for 1000 h–4000 h [9].

The 3D reconstructed images of the isolated-Ni phase on exposure to 40% H_2O–60% H_2 atmosphere at 1000 °C, 1100 °C, and 1200 °C for 50 h are displayed in Fig. 6. The size of samples and the ratio of isolated-Ni phase to whole Ni phase are listed in Table 2. Because the volume ratio of Ni to YSZ in each sample was almost unity as shown in Table 1, it was confirmed that the rectangular specimen was large enough. The red regions (in the web version) correspond to the isolated-Ni phase in Fig. 6. The isolated-Ni phase is defined as the phase which is unconnected to the any surfaces of anode samples. The isolated Ni phase apparently became quite large at 1200 °C. The rate of isolated-Ni phase increased with a rise in treatment temperature, which corresponds to the decrease in effective electronic conduction path. Because this tendency was related to the performance of heat-treated Ni–YSZ anodes, the interruption of electronic conduction path and the concomitant reduction in electrochemical reaction sites should be one reason of the performance deterioration of Ni–YSZ anodes.

Table 1
Volume fraction evaluated from the reconstructed anode microstructures of Ni–YSZ before treatment and after holding at OCV for 50 h.

	Phase	Initial [21]	1000 °C 40% H_2O	1100 °C 10% H_2O	1100 °C 40% H_2O	1200 °C 40% H_2O
Volume fraction%	Ni	25.3	28.6	26.4	26.9	23.9
	YSZ	25.1	20.5	22.7	22.6	22.8
	Pore	49.6	50.9	50.9	50.2	53.3

The triple phase boundary (TPB) length could be also calculated from the 3D microstructure of the anodes. The active TPB length was estimated after removing the isolated parts of Ni, YSZ and pore from the whole reconstructed model. Table 3 shows total TPB and active TPB lengths for Ni–YSZ anodes after heat-treatments. Both TPB lengths were reduced with a rise in humidity and temperature, which resulted from the sintering of Ni particles shown in Fig. 5(b). Note that the high humidity lowered the TPB length of anodes only slightly at 1100 °C. On the contrary, the deterioration rate of anode performance (see in Fig. 2) was strongly affected by the humidity in the treatment atmospheres. Accordingly, the decrease in active TPB length is not the decisive factor to cause the degradation of cell performance.

Throughout this study, it could be concluded that the deterioration of anode performance under high humidity and temperature conditions would be attributable to the progress in the crack formation in the layer rather than the reduction in TPB length.

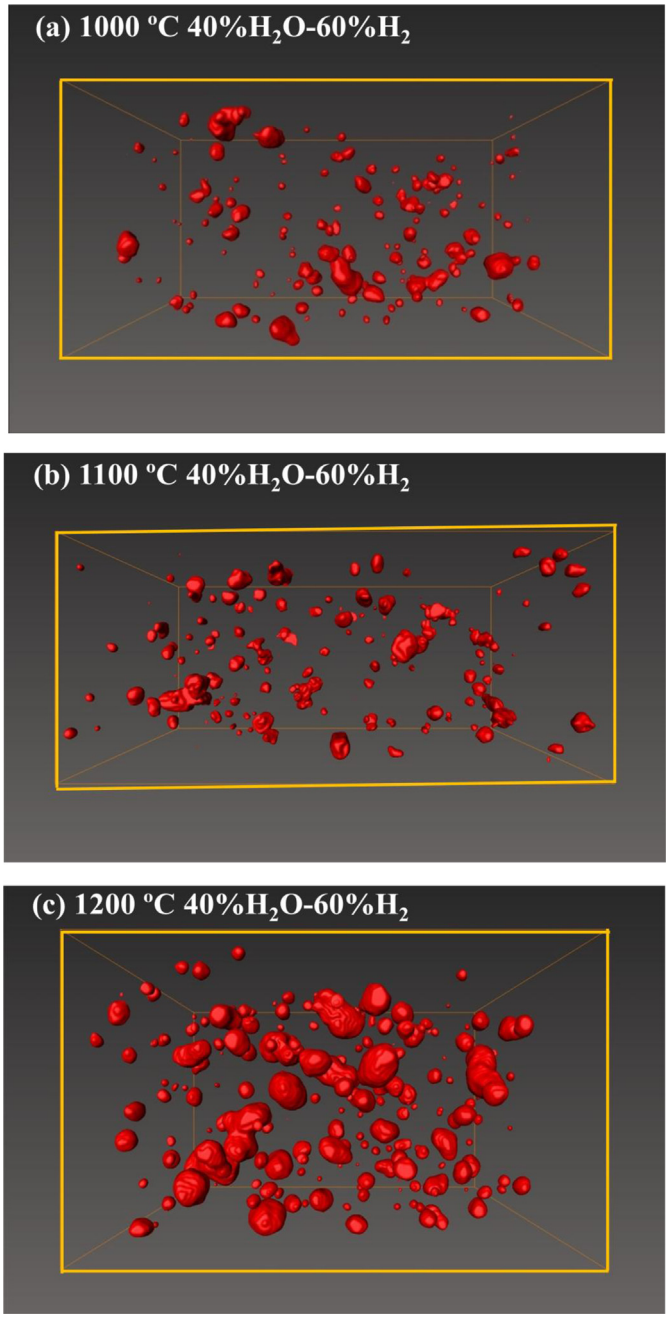

Fig. 6. 3D reconstructed isolated Ni phases for Ni–YSZ anode after flowing 40% H_2O–60% H_2 for 50 h at (a) 1000 °C, (b) 1100 °C, and (c) 1200 °C.

Table 2
Sizes and isolated-Ni phase ratio of anode before treatment and after holding at OCV for 50 h.

	Direction	Initial [21]	1000 °C 40% H_2O	1100 °C 40% H_2O	1200 °C 40% H_2O
Dimension/μm	*x*	25.77	29.01	29.03	24.22
	y	11.62	12.01	14.04	15.30
	z	6.57	17.67	20.71	22.63
Isolated-Ni phase ratio		3.8%	4.0%	6.6%	9.0%

Table 3
Triple phase boundary (TPB) length and active TPB length for Ni–YSZ anode before treatment and after holding at OCV for 50 h.

Ni–YSZ anode	Initial [21]	1000 °C 40% H_2O	1100 °C 10% H_2O	1100 °C 40% H_2O	1200 °C 40% H_2O
Total TPB length (μm/μm^3)	2.49	1.76	1.47	1.30	1.11
Active TPB length (μm/μm^3)	2.02	1.51	1.24	1.17	0.87

3.3. Mechanism of Ni coarsening

The migration mechanism of Ni particles under humidity conditions was discussed by several researchers [11–13]. The aggregation of Ni particles proceeds easily at high temperatures with high humidity. According to thermodynamic equilibrium, Ni species formed significantly under higher H_2O concentration. Therefore, several researchers suggested that Ni became Ni-hydroxide complexes readily under high humidity atmosphere to accelerate sintering of Ni particles via vapor transport mechanism [11–13]. However, the thermodynamic equilibrium suggests that diffusion of Ni-hydroxide complexes (i.e. $Ni(OH)_{2(g)}$) no significantly increased even at 1200 °C under the 40% H_2O–60% H_2 atmosphere. It is hard to ascribe that Ni evaporation is the main reason of Ni agglomeration, leading to anodic performance degradation. Hauch et al. also suggested this opinion [7]. We consider another mechanism of Ni atoms transportation under high humidity atmosphere.

In this study, we observed that some YSZ particles were surrounded by the Ni particles especially after holding under 40% H_2O–60% H_2 atmosphere at 1200 °C as shown in Fig. 7. The gray region was attributed to YSZ by EDX analysis, and the white region to Ni. In addition, Holzer et al. studied that the sintering of Ni particles in the Ni–GDC cermet during discharge at 950 °C for long-term operation [13]. The formation of a continuous GDC layer surrounded by the Ni particles was observed obviously after exposure to 3% H_2O–12% H_2–85% N_2 for 2286 h with discharge at 0.87 V. Ni particles appear to migrate along YSZ or GDC particle surface to result in this phenomenon. Therefore, we consider that steam concentration in the vicinity of TPB is relatively higher than

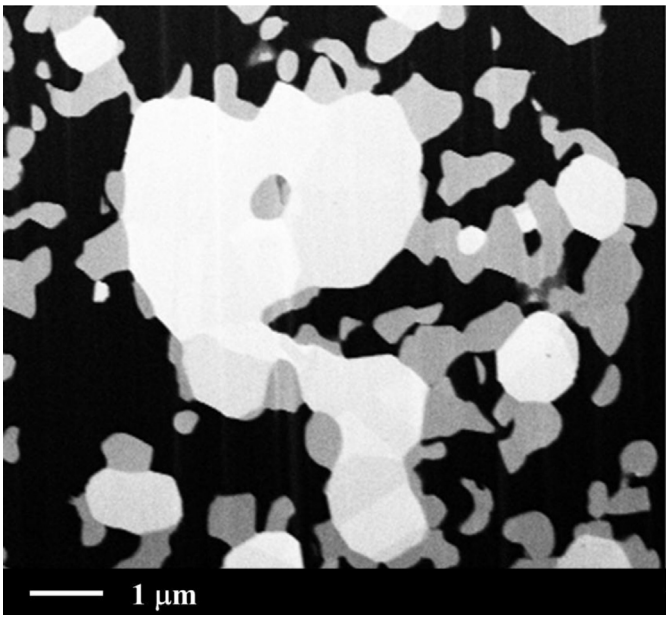

Fig. 7. FIB–SEM images for Ni–YSZ anode after holding at OCV for 50 h with a supply of 40% H_2O–60% H_2 at 1200 °C.

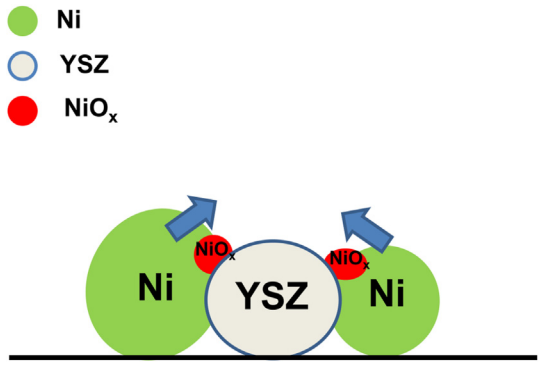

Fig. 8. Schematic of Ni particle agglomeration.

on the Ni particle surface under high humidity atmosphere. Thus, the surface of Ni may generate Ni oxide more readily near TPBs as shown in Fig. 8. Moreover, it has been considered that Ni-ion can migrate outward though NiO_x [22]. Ni particles may move along YSZ or GDC particle gradually, and finally be combined into one bigger particle.

4. Conclusions

The microstructural changes of Ni–YSZ anodes after heat-treat were quantitatively evaluated by FIB–SEM analysis. According to these results, the growth of Ni particles proceeded with increasing temperature and humidity condition, leading to the degradation of anode performance. The isolated-Ni phase grew with progress in sintering of Ni particles, inducing interruption of electronic conduction path and reduction of electrochemical reaction sites. The total and active TPB lengths also reduced with a rise of humidity and temperature. Detrimental deterioration of anode performance has been resulted from obvious generation of cracks observed on the surface and in the layers of the anode at higher humidity and temperature. On exposure to 40% H_2O–60% H_2 at 1200 °C for 50 h, the Ni–YSZ anode was separated into several island-like segments which restrict the ionic and electronic conductions in the in-plane direction of anode layer. In this study, the degradation of anode performance would be attributable to the propagation of the crack formation in the layer.

Acknowledgment

This work was supported by New Energy and Industrial Technology Development Organization (NEDO), Japan (Development of System and Elemental Technology on Solid Oxide Fuel Cell).

References

[1] S.M. Haile, Acta Mater. 51 (2003) 5981–6000.
[2] B.C.H. Steele, A. Heinzel, Nature 414 (2001) 345–352.
[3] S. McIntosh, R.J. Gorte, Chem. Rev. 104 (2004) 4845–4865.
[4] M. Vogler, Anja Bieberle-Hütter, Ludwig Gauckler, Jürgen Warnatz, Wolfgang G. Besslera, J. Electrochem. Soc. 156 (5) (2009) B663–B672.
[5] J. Mizusaki, H. Tagawa, T. Saito, T. Yamamura, Solid State Ionics 70/71 (1994) 52–58.
[6] S.P. Jiang, J. Mater. Sci. 38 (2003) 3775–3782.
[7] A. Hauch, M. Mogensen, A. Hagen, Solid State Ionics 192 (2011) 547–551.
[8] J.S. Cronin, J.R. Wilson, S.A. Barnett, J. Power Sources 196 (2011) 2640–2643.
[9] D. Simwonis, F. Tietz, D. Stöver, Solid State Ionics 132 (2000) 241–251.
[10] P. Tanasini, M. Cannarozzo, P. Costamagna, A. Faes, J.V. Herle, A. Hessler-Wyser, C. Comninellis, Fuel Cells 09 (2009) 740–752.
[11] J. Sehested, J.A.P. Gelten, I.N. Remediakis, H. Bengaard, J.K. Nørskov, J. Catal. 223 (2004) 432–443.
[12] L. Holzer, B. Iwanschitz, Th. Hocker, B. Munch, M. Prestat, D. Wiedenmann, U. Vogt, P. Holtappels, J. Sfeir, A. Mai, Th. Graule, J. Power Sources 196 (2011) 1279–1294.
[13] J. Sehested, Catal. Today 111 (2003) 103–110.
[14] M. Kishimoto, H. Iwai, M. Saito, H. Yoshida, J. Power Sources 196 (2011) 4555–4563.
[15] N. Vivet, S. Chupin, E. Estrade, T. Piquero, P.L. Pommier, D. Rochais, E. Bruneton, J. Power Sources 196 (2011) 7541–7549.
[16] J.R. Wilson, M. Gameiro, K. Mischaikow, W. Kalies, P.W. Voorhees, S.A. Barnett, Microsc. Microanal. 15 (2009) 71–77.
[17] T. Matsui, J.-Y. Kim, H. Muroyama, M. Shimazu, T. Abe, M. Miyao, K. Eguchi, Solid State Ionics 225 (2012) 50–54.
[18] N. Shikazono, D. Kanno, K. Matsui, H. Teshima, S. Sumino, N. Kasagi, J. Electrochem. Soc. 157 (5) (2010) B665–B672.
[19] Y.-H. Lee, H. Sumi, H. Muroyama, T. Matsui, K. Eguchi, J. Electrochem. Soc. 160 (6) (2013) F579–F584.
[20] H. Iwai, N. Shikazono, T. Matsui, H. Teshima, M. Kishimoto, R. Kishida, D. Hayashi, K. Matsuzaki, D. Kanno, M. Saito, H. Muroyama, K. Eguchi, N. Kasagi, H. Yoshida, J. Power Sources 195 (2010) 955–961.
[21] T. Matsui, R. Kishida, H. Muroyama, K. Eguchi, J. Electrochem. Soc. 159 (8) (2012) F456–F460.
[22] D. Sarantaridis, R.J. Chater, A. Atkinson, J. Electrochem. Soc. 155 (5) (2008) A467–A472.